The adenosine 2a receptor and TIM3 directly inhibit killing of tumor cells by cytotoxic T lymphocytes through interference with cytoskeletal polarization

Grace L. Edmunds [1], Carissa C.W. Wong [1], Rachel Ambler [1], Emily Milodowski [1], Hanin Alamir [1], Stephen J. Cross [2], Gabriella Galea [1], Christoph Wülfing [1, 3, *], David J. Morgan [1, 3, *]

1 School of Cellular and Molecular Medicine, University of Bristol, United Kingdom
2 Wolfson BioImaging Facility, University of Bristol, United Kingdom
3 equal contribution

* Email: Christoph.Wuelfing@bristol.ac.uk; D.J.Morgan@bristol.ac.uk

Abstract

Tumors generate an immune-suppressive environment that prevents effective killing of tumor cells by $CD8^+$ cytotoxic T cells (CTL). It remains largely unclear upon which cell type and at which stage of the anti-tumor response mediators of suppression act. We have combined an *in vivo* tumor model with a matching *in vitro* reconstruction of the tumor microenvironment based on tumor spheroids to identify suppressors of anti-tumor immunity that directly act on interaction between CTL and tumor cells and to determine mechanisms of action. An adenosine 2a receptor antagonist, as enhanced by blockade of TIM3, slowed tumor growth *in vivo.* Engagement of the adenosine 2a receptor and TIM3 reduced tumor cell killing in spheroids, impaired CTL cytoskeletal polarization *ex vivo* and *in vitro* and inhibited CTL infiltration into tumors and spheroids. With this focus on CTL killing, blocking A2aR and TIM3 complements therapies that enhance T cell priming, e.g. anti-PD1 and anti-CTLA-4.

Introduction

$CD8^+$ cytotoxic T cells (CTL) have the ability to directly kill tumor target cells. Such killing requires: effective priming of tumor antigen-specific $CD8^+$ T cells within the draining lymph nodes; differentiation into CTL; effective tumor infiltration and execution of the cytolytic effector function within the tumor microenvironment. However, solid tumors often generate an immune-suppressive environment with multiple often redundant immune-suppressive elements that prevent effective tumor cell killing. For the development of widely applicable curative cancer immunotherapies multiple reagents with defined mechanisms of action that can be flexibly combined are required, at least some of which need to restore CTL killing within the tumor (1). Here we have characterized two such reagents.

Inhibitory receptors, in particular CTLA-4, PD-1, TIGIT, TIM3 and LAG3, impair the anti-tumor immune response (2, 3). Blocking CTLA-4 and PD-1 is a cornerstone of current immunotherapy and has yielded great therapeutic success in many cancer types (4). However, efficacy is limited to a subset of patients and few tumor types, and autoimmune side effects can be substantial. Mechanisms of action of PD-1 blockade are still being debated. Initially, it was widely assumed that blocking PD-1 would reactive tumor-infiltrating CTL (TIL) that had acquired a suppressed state characterized by enhanced PD-1 expression. However, PD-1 and also CTLA-4 are expressed not only on CTL but also on other T cell subtypes, other immune cell types and even on tumor cells. Deletion of PD-1 in myeloid cells can enhance anti-tumor immunity more effectively than deletion in T cells (5). In basal or squamous cell carcinoma patients, PD-1 blockade does not reactivate tumor-resident CTL but leads to infiltration of new CTL clones (6). We have shown that treating mice with anti-PD-1 enhances anti-tumor immunity but treating TIL directly *ex vivo* does not enhance their function (7), further arguing for an effect independent of the direct CTL tumor cell interaction. Ligands of CTLA-4 are expressed on antigen presenting cells in T cell priming but not commonly on tumor cells. Therefore, CTLA-4 blockade is more likely to enhance T cell priming rather than reactivate TIL. Potential depletion of regulatory T cells by anti-CTLA-4, even though controversial, can also be expected to affect priming (8-10). The effects of PD-1 and CTLA-4 blockade on T cell priming may be critical in the development of autoimmune side effects by allowing self-reactive T cells to activate. PD-1 and CTLA-4 blockade are most effective in patients that already have tumors with a substantial immune infiltrate rich in $CD8^+$ T cells (11), limiting the applicability of PD-1 and CTLA-4 blockade across many cancer types. Thus, means to enhance anti-tumor immunity that focus more strongly on (re)activation of CTL and/or enhancing tumor infiltration rather than on the priming of new T cell clones are of substantial interest in the development of a diverse combinatorial tool kit for curative cancer immunotherapy.

Key soluble mediators of tumor-mediated immune suppression are adenosine and prostaglandin E2 (PGE_2). Both use an increase in intracellular cyclic AMP (cAMP) as a key signaling mechanism and may, therefore, have overlapping functions (12, 13). PGE_2 strongly regulates dendritic cell biology and thus T cell priming (14). Adenosine is generated by hydrolysis of extracellular ATP by the ectoenzymes CD39 and CD73 (15) the expression of which is increased in hypoxic and immunosuppressive tissue environments (16). Adenosine concentrations are therefore greatly enhanced in the tumor microenvironment (12, 17). Adenosine signals through a family of four adenosine receptors (12, 13). The adenosine ADORA 2A receptor (A2aR) is highly expressed in T cells. A2aR blockade or T cell-specific

deletion enhance anti-tumor immunity in many models, often with enhanced CTL tumor infiltration (18-21). The localized generation of adenosine and its role in tumor infiltration make adenosine an attractive target as a regulator of tumor immunity with a direct focus on the tumor microenvironment.

Expression of the inhibitory receptor TIM3 increases with repeated T cell stimulation (22) reaching particularly high levels in tumors. High TIM3 expression in tumors is related to poor overall survival (23). Blocking TIM3 can enhance anti-tumor immunity, in particular in combination with anti-PD-1 or chemotherapy (24). While TIM3 is highly expressed on $CD8^+$ TIL, TIM3 also regulates myeloid cell function , is highly expressed on $CD4^+$ Tregs in tumors and TIM3 signaling can display features of costimulation, such as activation of Akt/mTor (25, 26). Even though the mechanism of action of TIM3 thus remains unresolved, its preferential expression on $CD8^+$ TIL makes it an attractive candidate for a direct regulator of the interaction between CTL and their tumor target cells.

Here we aim to determine whether effectors of tumor-mediated immune suppression can directly regulate the killing of tumor target cells by CTL. We complement an *in vivo* tumor model with a matching *in vitro* reconstruction of the tumor microenvironment based on the interaction of tumor spheroids with CTL in the absence of any other cell types (7, 27, 28): Murine renal carcinoma cells expressing the hemagglutinin (HA) protein from influenza virus A/PR/8 as neo-tumour-specific antigen (RencaHA) are effectively recognized by the immune system *in vivo* and generate an immune-suppressive tumor microenvironment. Recognition of Renca tumors can be enhanced with adoptive transfer of CL4 T cell receptor transgenic CTL recognizing an HA-derived peptide. *In vitro*, RencaHA cells cultured in three-dimensional spheroids effectively interact with CL4 CTL such that the suppressed phenotype acquired in this *in vitro* interaction closely matches that acquired by adoptively transferred CL4 CTL *in vivo* (7*)*. A key element of the mechanism of the impaired killing ability of tumor-suppressed CTL is the reduced ability of CTL to execute the cytoskeletal polarization steps required for effective target cell killing (7).

Blocking A2aR partially reduced RencaHA tumor growth *in vivo*. Upon A2aR blockade TIM3 was highly upregulated amongst $CD8^+$ TIL. Combing *in vivo* blockade of A2aR with that of TIM3 further reduced tumor growth in the context of adoptive transfer of CL4 T cells. This combined treatment partially restored the ability of CTL to polarize towards their tumor target cells and enhanced tumor infiltration of CTL. *In vitro*, overexpression of TIM3 by CL4 CTL and treatment with an A2aR agonist inhibited killing of tumor cells in tumor spheroids and the A2aR agonist also reduced spheroid infiltration by CTL. An A2aR agonist suppressed cytoskeletal polarization of CTL during both migration and coupling to tumor target cells. Interference with cytoskeletal polarization thus is a mechanism by which A2aR and TIM3 directly suppress killing of tumor cells by CTL.

Results

An experimental approach to identify direct suppressors of CTL killing of tumor target cells

Enhancing the ability of CTL to kill tumor target cells within the tumor microenvironment (TME) is of immense therapeutic interest. To identify immunosuppressive factors that act directly on CTL within the TME, we combined *in vivo* mouse studies with matched direct investigation of the interaction of CTL with tumor spheroids *in vitro* (Fig. 1)(7, 27, 28): Renca renal carcinoma cells expressing influenza A/PR/8/H1N1 hemagglutinin (HA) induce an endogenous anti-tumor immune response and an immune-suppressive TME when grown subcutaneously in mice. The T cell receptor (TCR) of T cells from CL4 TCR transgenic mice recognizes the HA peptide 518 to 526 (IYSTVASSL) as restricted by H2-K^d. Upon adoptive transfer into RencaHA tumor-bearing mice, CL4 CTL infiltrate the tumor and acquire a suppressed phenotype (7). Incubation of *in vitro* primed CL4 CTL with RencaHA tumor cells grown as three-dimensional spheroids induces a suppressed CTL phenotype that shares key features with tumor-infiltrating CL4 T cells (7). Thus, we could characterize tumor-associated immunosuppression of CD8$^+$ T cells in parallel in the *in vivo* tumor model to establish physiological relevance and in the *in vitro* spheroids to establish direct effects on the interaction of CTL with tumor cells in the absence of other immune cells.

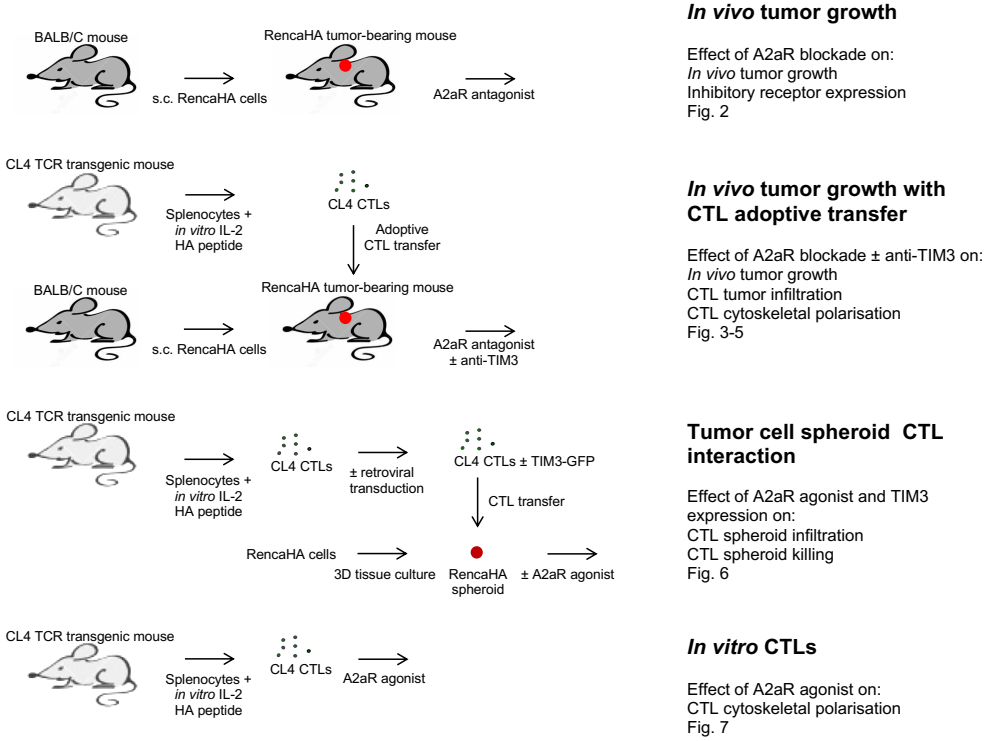

Figure 1 – Schematic representation of the experimental system.

The adenosine 2a receptor suppresses anti-tumor immunity

High concentrations of adenosine occur within many solid tumors. $CD4^+FoxP3^+$ regulatory T cells (Tregs) express the adenosine-generating ectoenzymes CD39 and CD73 as an important means of *in situ* adenosine generation. Within TIL from RencaHA tumor-bearing mice 86±2% of $CD25^+FoxP3^+CD4^+$ T cells expressed both CD39 and CD73 (Fig. 2A). $CD25^+CD4^+$ TIL from RencaHA tumor-bearing mice suppressed *in vitro* proliferation of naïve CL4 T cells in a manner dependent on the adenosine 2a receptor (A2aR)(Fig. 2B). This *in vitro* generation of functionally relevant amounts of adenosine by $CD25^+FoxP3^+CD4^+$ TIL suggests that these cells can also generate elevated adenosine concentrations in the RencaHA TME.

To determine whether A2aR suppresses anti-tumor immunity in the RencaHA model, we treated RencaHA tumor-bearing mice with the A2aR antagonist ZM 241385 (Fig. 1)(29, 30). Under control conditions, tumors grew from 150±25mm^3 at day 12, the start of treatment, to 2075±290mm^3 within eight days with two mice sacrificed early as their tumors exceeded maximum allowable tumor volume. ZM 241385 treatment resulted in a reduction in tumor growth from 140±35mm^3 to only 715±85mm^3 over eight days with no mice needing to be sacrificed ($p<0.01$)(Fig. 2C). These data establish a partial role of A2aR in suppressing anti-tumor immunity in the RencaHA model.

TIM3 expression is enhanced on CTL upon *in vivo* A2aR blockade

The only partial nature of the suppression of tumor growth upon A2aR blockade suggest that other elements of tumor-mediated immune suppression may synergize with A2aR engagement or are even upregulated to compensate for A2aR blockade. We, therefore, determined the expression of inhibitory receptors: TIM3, TIGIT, LAG3, PD-1, and adenosine-producing ectoenzymes: CD39 and CD73 by both $CD8^+$ and $CD4^+$ TIL from ZM 241385-treated and control tumors.

To identify combinations of inhibitory receptor expression altered upon A2aR blockade, we used a principal component analysis. Input data were percentage of T cells expressing inhibitory receptors in all combinations and tumor size (Fig. 2D, E). Principal component (PC) 1 effectively distinguished TIL from ZM 241385-treated and control mice (95% confidence ellipses are shown). Variables which contribute to PC1 were therefore positively associated with A2aR antagonism of TIL. TIM3 expression was significantly upregulated in combination with other inhibitory receptors by A2aR-antagonist treatment and contributed to PC1 with $p<0.001$. PD-1 and TIGIT expression were also strongly associated with PC1, albeit TIGIT both amongst drivers and opposers. Thus, upregulation of the expression of PD-1 and TIM3 is most strongly associated with A2aR blockade. As TIM3 is more likely to directly affect the interaction of CTL with their tumor cell targets as discussed in the introduction, we selected TIM3 blockade as an adjunct treatment to improve responses to A2aR-antagonism. Expression of various combinations of inhibitory receptors by $CD4^+$ TIL was also associated with A2aR-antagonist treatment, as not further pursued here because of our focus on the direct interaction between $CD8^+$ CTL and tumor target cells.

PC2 separated TIL by the volume of the tumor they are derived from, with larger tumors associating positively with PC2. This highlights the importance of accounting for tumor volume when assessing immune profiles. CD39 expression strongly drove PC2 while opposing PC1. This indicates that with increasing size control tumors relied more on adenosine for

immune suppression as opposed by A2aR antagonism. Only in the largest tumors, >1,000mm^3, did inhibitory receptor expression in TIL start to increase as an additional suppressive mechanism (Fig. S1). Conversely, amongst A2aR-blocked tumors, TIL inhibitory receptor expression was already high in smaller tumors, providing an alternate means of suppression in the absence of A2aR (Fig. S1). Together these data suggest that RencaHA tumors rely strongly on A2aR for immune suppression with compensatory upregulation of inhibitory receptor expression upon A2aR blockade.

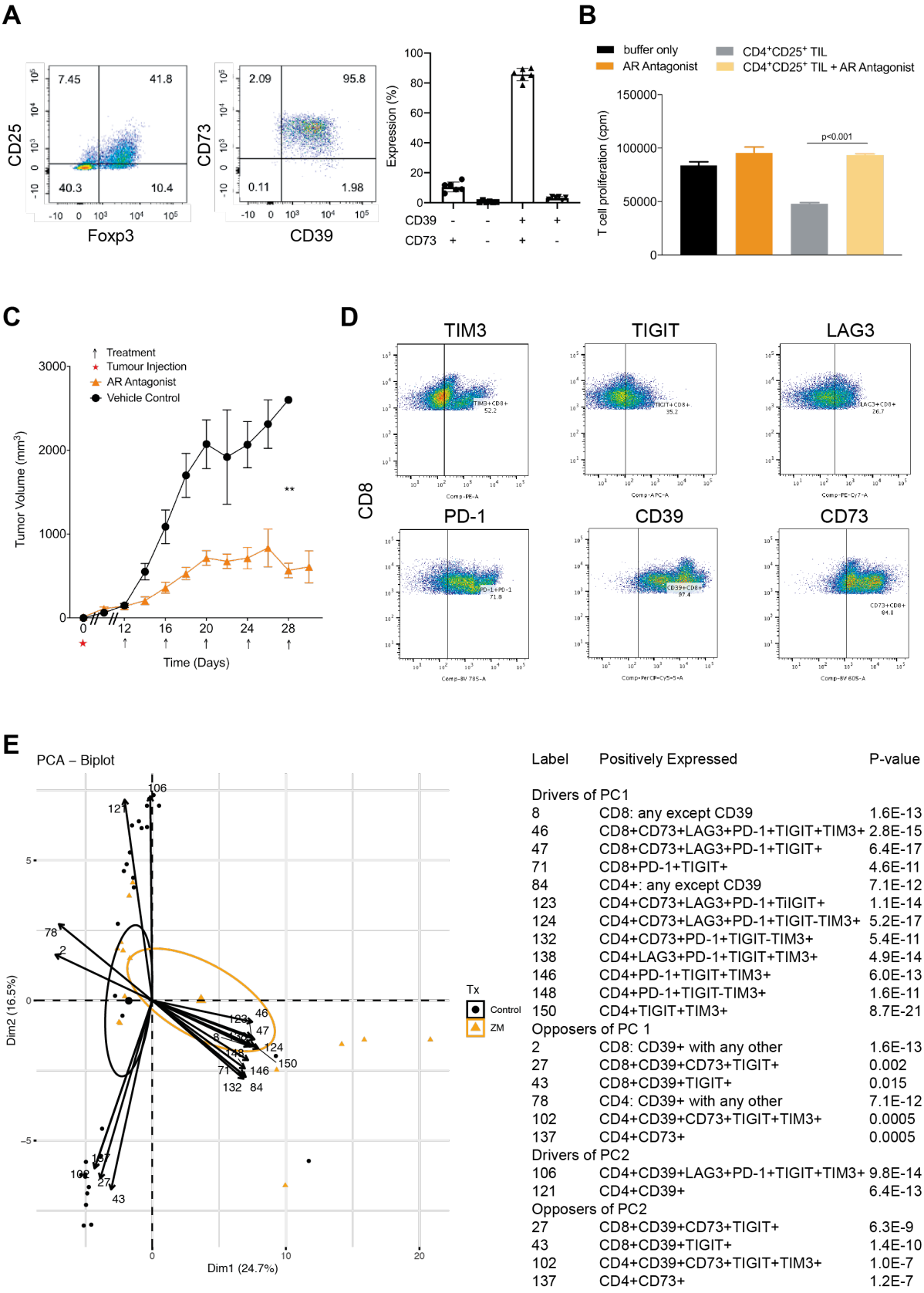

Label	Positively Expressed	P-value
Drivers of PC1		
8	CD8: any except CD39	1.6E-13
46	CD8+CD73+LAG3+PD-1+TIGIT+TIM3+	2.8E-15
47	CD8+CD73+LAG3+PD-1+TIGIT+	6.4E-17
71	CD8+PD-1+TIGIT+	4.6E-11
84	CD4+: any except CD39	7.1E-12
123	CD4+CD73+LAG3+PD-1+TiIGIT+	1.1E-14
124	CD4+CD73+LAG3+PD-1+TIGIT-TIM3+	5.2E-17
132	CD4+CD73+PD-1+TIGIT-TIM3+	5.4E-11
138	CD4+LAG3+PD-1+TIGIT+TIM3+	4.9E-14
146	CD4+PD-1+TIGIT+TIM3+	6.0E-13
148	CD4+PD-1+TIGIT-TIM3+	1.6E-11
150	CD4+TIGIT+TIM3+	8.7E-21
Opposers of PC 1		
2	CD8: CD39+ with any other	1.6E-13
27	CD8+CD39+CD73+TIGIT+	0.002
43	CD8+CD39+TIGIT+	0.015
78	CD4: CD39+ with any other	7.1E-12
102	CD4+CD39+CD73+TIGIT+TIM3+	0.0005
137	CD4+CD73+	0.0005
Drivers of PC2		
106	CD4+CD39+LAG3+PD-1+TIGIT+TIM3+	9.8E-14
121	CD4+CD39+	6.4E-13
Opposers of PC2		
27	CD8+CD39+CD73+TIGIT+	6.3E-9
43	CD8+CD39+TIGIT+	1.4E-10
102	CD4+CD39+CD73+TIGIT+TIM3+	1.0E-7
137	CD4+CD73+	1.2E-7

Figure 2 – An A2aR antagonist delays *in vivo* tumor growth and triggers compensatory upregulation of T cell inhibitory receptors

A TIL from RencaHA tumor-bearing BALB/c mice were stained with anti-CD25, anti-FoxP3, anti-CD39 and anti-CD73 mAb. On the left and in the middle, representative flow cytometry data are shown. On the right, percentage TIL expressing CD39 and CD73 are given as mean ± SEM for N=6 experiments. **B** $CD4^+CD25^+$ TIL from RencaHA tumor-bearing BALB/c mice were co-cultured with naïve $CD8^+$ CL4 T cells and irradiated mature dendritic cells and K^dHA peptide with or without the A2aR antagonist ZM 241385 at 1.25 µM for 3 days. ^{3}H-thymidine incorporation (cpm) is shown as mean ± SEM. N=10 mice over two experiments (paired t-test). **C** Mean RencaHA tumor volume is given in BALB/c mice after s.c. injection of 1 x 10^6 RencaHA tumor cells on day 0 and i.p. injection with ZM 241385 when tumors had reached 5 mm diameter in any one direction (day 12-14) and further treatments administered every other day as indicated (linear mixed model to perform repeated measures ANOVA. ** is $p<0.01$). N=26 treated mice and 20 control mice over 4 separate experiments. **D** $CD45^+$ cells from the RencaHA tumor bearing mice in B were stained using mAbs against CD8, CD4, CD39, CD73, TIM3, TIGIT, LAG3 and PD-1. Representative flow cytometry data are shown. **E** The outcome of a principal component analysis is given with input data of percentage expression of markers in D in each combination of the eight markers, representing 308 variables , and tumor volume as an additional variable. Each triangle (ZM 241385-treated) or circle (control-treated) represents an individual tumor-bearing mouse. Large symbols represent the average position of treated and control mice along PC1 with ellipses showing 95% confidence intervals. The 24 variables making the greatest contribution to principal component (PC) 1 and 2 are overlaid as numbered vectors and are listed in the table.

TIM3 enhances suppression of $CD8^+$ T cell-dependent anti-tumor immunity by A2aR

To investigate immunosuppressive synergy between A2aR and TIM3, groups of BALB/c mice bearing 12 day old RencaHA tumors were treated with the A2aR antagonist ZM 241385 plus or minus the anti-TIM3 blocking mAb RMT3-23 (Fig. 1). For precise temporal synchronization and a standardized number of anti-tumor CTL, we used i.v. double adoptive T cell transfer (ATT) of 5x10^6 CL4 TCR transgenic CTL on days 12 and 14. We observed three phases of tumor growth upon treatment, an initial 'growth' phase of six days, a 'response' phase of eight days and a subsequent open ended 'relapse' phase (Fig. 3A). As an overall outcome measure, we determined a ratio of the final tumor volume after growth, response and relapse to initial tumor volume at the start of treatment. Adoptive transfer of CL4 CTL plus both ZM 241385 and anti-TIM3 mAb gave a significant ($p<0.05$) reduction in the average final to initial tumor volume ratio compared with mice receiving adoptive CL4 T cell transfer plus ZM 241385 only. TIM3 thus enhances suppression of anti-RencaHA tumor immunity by A2aR (Fig. 3B).

To determine at which stage of tumor growth treatment with ZM 241385 and anti-TIM3 mAb exerted its effect, we analyzed the three phases of tumor growth separately. Initial tumor growth in all mice peaked between day 14-18. The combination of adoptive transfer of CL4 CTL with both ZM 241385 and anti-TIM3 mAb resulted in a marked reduction in tumor growth relative to mice given either CL4 T-cells alone, or CL4 CTL plus ZM 241385 (Fig. 3C) suggesting that TIM3 enhances suppression of anti-RencaHA tumor immunity by A2aR already in this early phase of tumor growth.

In the 'response' phase, between days 20 and 26, most tumors regressed in all treatment groups. Comparing this regression to the continued RencaHA tumor growth in the absence of CL4 CTL adoptive transfer (Fig. 2C, 3A), the regression can be attributed to the transferred CL4 CTL. Mice in which tumors regressed were categorized as 'responders'. The percentage of responder mice didn't differ between the treatment groups (Fig. 3D). We then defined

'relapse' as tumors reaching a volume ≥ the starting volume. When analyzing all mice, relapse was slightly delayed in mice treated with ZM 241385 and anti-TIM3 mAb without reaching statistical significance (Fig. 3E). When analyzing relapse only in responders, relapse frequencies differed substantially with treatment. Upon adoptive transfer of CL4 CTL alone, 8/17 tumors relapsed within 26 days of regression. Upon treatment with adoptive transfer of CL4 CTL and ZM 241385, tumor relapse occurred in 8/10 responder mice. However, when anti-TIM3 mAb was used in combination with ZM 241385 plus adoptive transfer of CL4 CTL, only 3/12 mice underwent relapse after regression ($p<0.05$ compared to treatment with CL4 adoptive transfer plus ZM 241385). Thus, blocking A2aR together with TIM3 decreased RencaHA tumor relapse.

To elucidate mechanisms of the prevention of tumor relapse, we determined T cell persistence. After the initial response phase adoptively transferred Thy1.1$^+$ CL4 CTL were only detected in mice from the ZM 241385 plus anti-TIM3 mAb group. They could also be expanded by booster immunization with the HA peptide in mice receiving only CL4 CTL (Fig. 4A, S2A). However, Thy1.1$^+$ CL4 CTL were not detected in the group treated with ZM 241385 alone, with or without a booster immunization, consistent with the high relapse rate of 8/10. To determine the role of persistent CD8$^+$ T cells in tumor immunity, we depleted them. In mice with complete and durable tumor remission lasting >8 days, only 5 out of 19 mice experienced relapse (Fig. 4B). In addition, responder mice were resistant to tumor growth following rechallenge with tumor cells (Fig. 4C). In contrast, treatment with anti-Thy1.1 depleting mAb at 28 days induced tumor re-growth in 4/4 mice (Fig. 4D). Treatment with anti-CD8β depleting mAb resulted in tumor re-growth in 2/2 mice (Fig. 4E, S2B)($p<0.01$ of combined depletion data versus control). Together, these data establish that response and suppression of relapse depend on the continued presence of tumor-reactive CTL.

Thus far, our *in vivo* data establish that combined treatment with ZM 241385 and anti-TIM3 mAb enhances anti-tumor immunity in a T cell-dependent fashion. The mechanism underpinning the immune-enhancing effect of such treatment in the initial anti-tumor response is the focus of the remainder of this manuscript.

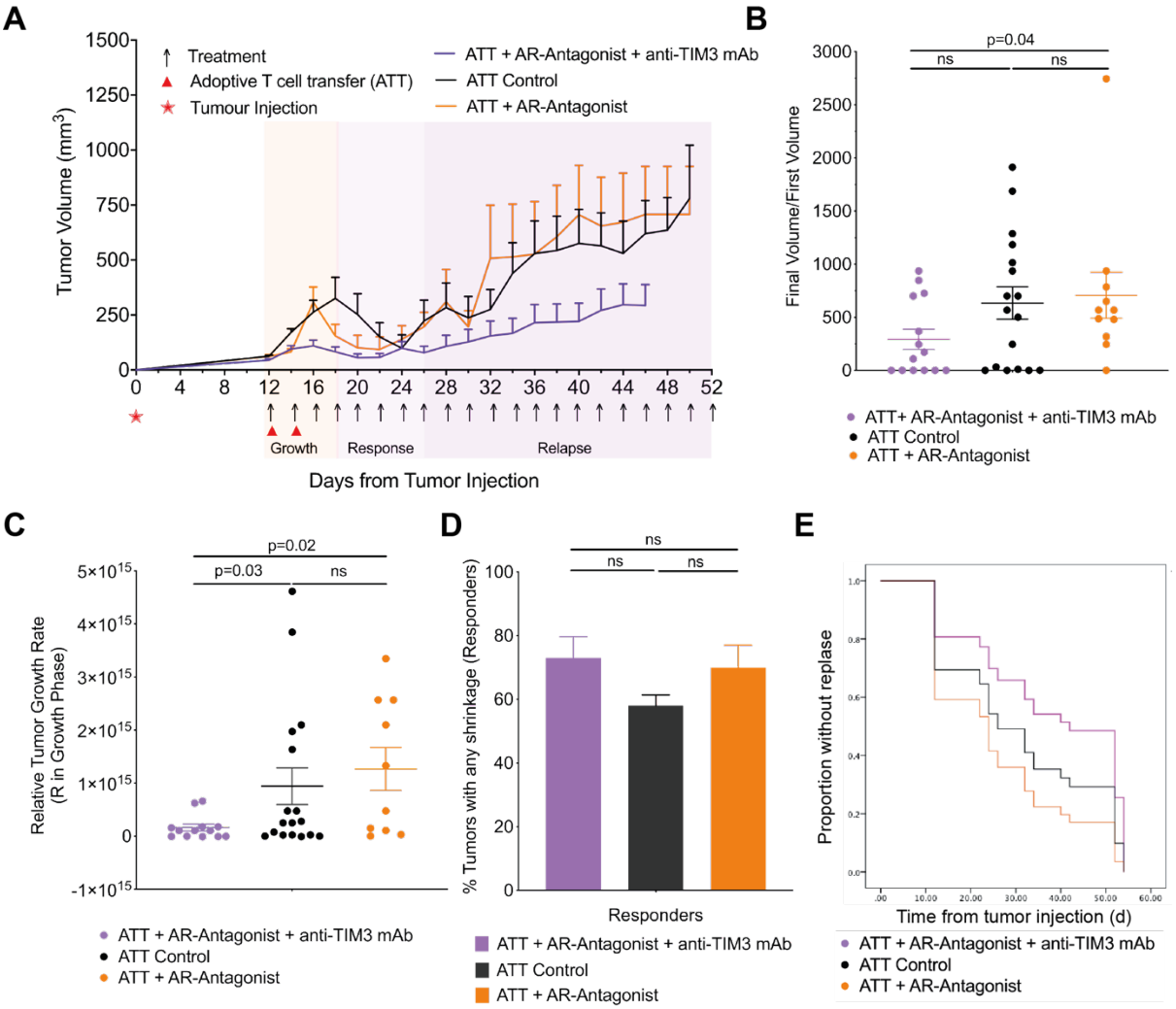

Figure 3 – A2aR antagonist and anti-TIM3 mAb synergistically suppress RencaHA tumor growth

A RencaHA tumor-bearing BALB/c mice were injected i.v. twice with 5 x10^6 purified CL4 CTL on days 12 and 14 and treated with AR-Antagonist, anti-TIM3 mAb, or vehicle + isotype-control antibody, as shown. Tumor growth is displayed as mean tumor volumes + SEM whith N=42 mice over 3 independent experiments, with at least 11 mice per group. **B** The ratio of final to initial (day 12) tumor volume of tumors in A is given (independent two sample t-test). **C** R values representing growth rate of tumors in A, between 12 and 16 days, are given (independent two sample t-test). **D** Proportion of tumors in A which were regressed are given. Fisher's exact Boschloo test. **E** Progression free survival of mice in A is given. Cox Proportional Hazards Regression analysis. Treatment did not significantly predict PFS: (p=0.24 ATT control; p=0.40 ATT + AR-Antagonist; p=0.30 ATT + AR-Antagonist + Anti-TIM3 mAb). Hazard ratio of progression versus Control was as follows: ATT + AR-Antagonist = 0.36 (0.61 ± 3.38), ATT + AR-Antagonist + Anti-TIM3mAb = - 0.53 (0.21 ± 1.63).

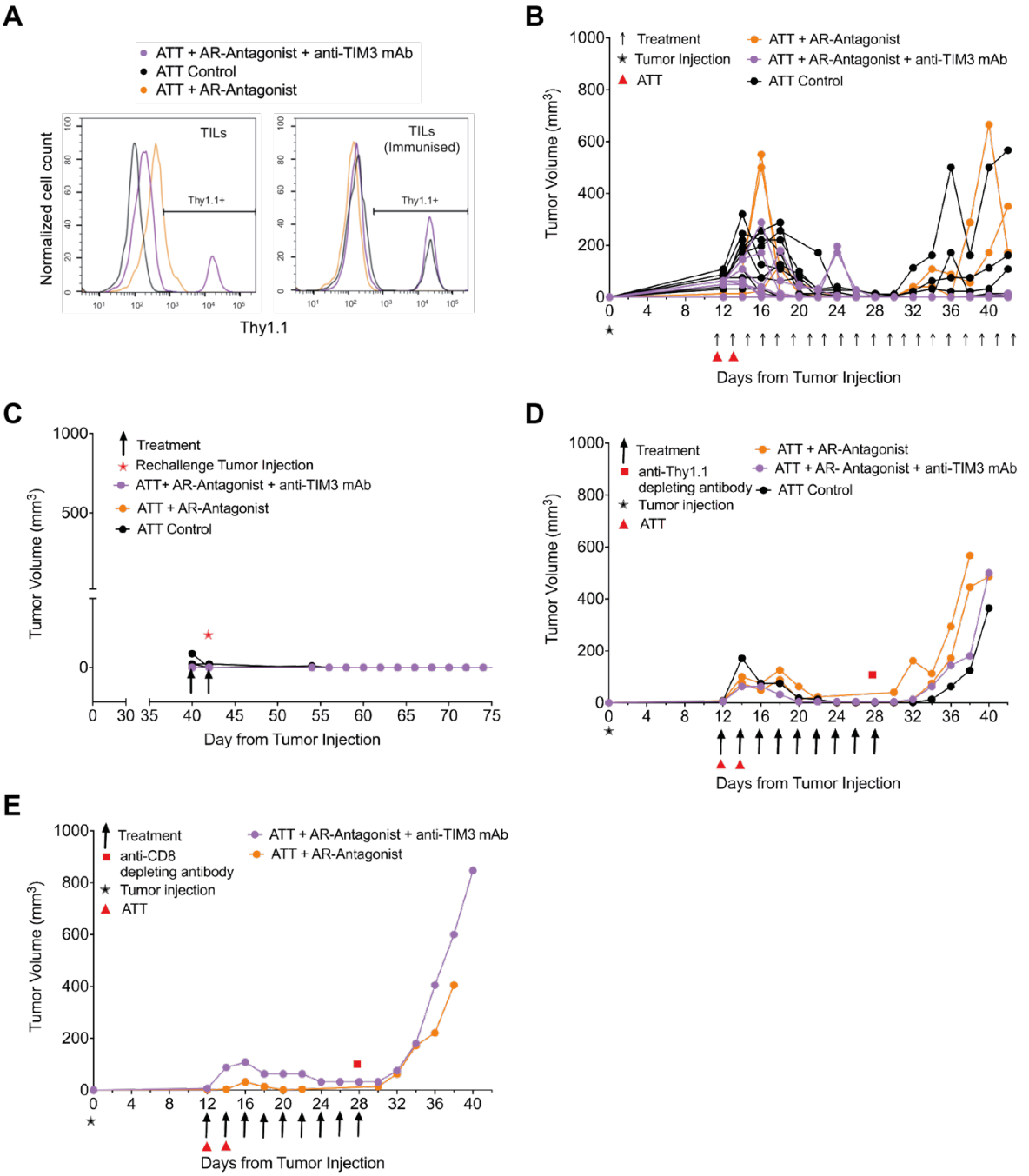

Figure 4 – A2aR antagonist plus anti-TIM3 mAb diminish tumor relapse in a T cell-dependent fashion

Mouse numbers across the different parts of the experiments are detailed in Fig. S2A. **A** RencaHA tumor-bearing BALB/c were injected i.v. with two doses of 5 x 10^6 Thy1.1$^+$ CL4 CTL (ATT) plus either vehicle and isotype control, Aa2R-Antagonist (ZM 241385) alone or A2aR-antagonist + anti-TIM3 mAb as shown. The percentage of Thy1.1$^+$ CL4 TIL between days 25 and 48 is given as representative data from N=25 mice over 3 independent experiments. Mice were either immunized with HA peptide 5 days prior to TIL harvest (N=5) to induce expansion of Thy1.1+ CL4 T cells or immunized with empty vehicle control (N=19); one representative graph is shown for each group. **B-E** Tumor growth curves from individual mice treated in Fig. 3A, which had experienced complete and durable tumor remission. **B** untreated and **C** rechallenged with tumor cells at day 40; **D** depleted of Thy1.1$^+$ T cells using

anti-Thy1.1 depleting mAb at 28 days; **E** depleted of all $CD8^+$ T cells using anti-CD8β depleting mAb at 28 days with depletion efficiency shown in Fig. S2B.

A2aR and TIM3 suppress the cellular polarization of CTL and tumor infiltration

Mechanisms of A2aR and TIM3 in suppression of anti-tumor immunity are of interest. For effective tumor infiltration and tumor cell killing CTL need to undergo a series of cytoskeletal polarization steps. The inability to effectively execute such steps characterizes tumor-infiltrating CTL (7). To determine if A2aR and TIM3 regulate effective TIL polarization in the tumor microenvironment, we isolated TIL from RencaHA tumors and imaged their subsequent interaction with K^dHA peptide pulsed Renca cells *ex vivo*. One hallmark of defective cytoskeletal TIL polarization are CTL lamellae directed away from the cellular interface with the tumor target cell as to destabilize the cell couple (Fig. 5A). Less than 30% of *in vitro* primed control CL4 CTL display such lamellae even after 15min of cell contact, whereas all TIL from control-treated tumor do so within 7min (Fig. 5B). Following treatment of mice with the A2aR antagonist ZM 241385 plus blocking anti-TIM3 mAb off-interface lamellae formed later, with the median time of first off-interface lamellae formation delayed from 100s to 220s. 11% of cell couples didn't show any off-interface lamellae at all (Fig. 5B). Another hallmark of defective TIL cytoskeletal polarization is T cell translocation over the tumor cell surface away from the site of initial coupling (Fig. 5C). While almost completely absent in *in vitro* primed control CTL, 71±9% of TIL displayed such translocation (Fig. 5D, E). This frequency was significantly ($p<0.001$) reduced to 37±9% and 23±7% upon tumor treatment with ZM 241385 alone or in combination with anti-TIM3 mAb, respectively. Data from these restoration experiments establish that A2aR as enhanced by TIM3 contributes to the defective cytoskeletal polarization of TIL. Consistent with the importance of such CTL cytoskeletal polarization for cytolysis, treatment of tumors with the A2aR antagonist ZM 241385 plus blocking anti-TIM3 mAb significantly ($p=0.02$) enhanced *ex vivo* CL4 TIL killing (Fig. 5F, G). We have also seen restoration of CTL cytoskeletal polarization and killing upon treatment of RencaHA tumor-bearing mice with anti-PD-1 (7). It is now of interest whether or not A2aR and TIM3, in contrast to PD-1 (7), directly regulate the interaction between CTL and their tumor target cells.

As an additional process requiring cytoskeletal activity, we examined the infiltration of endogenous $CD8^+$ T cells and CL4 CTL into Renca tumors *in vivo*. Such infiltration was focused on peripheral tumor regions and was enhanced upon treatment with the A2aR antagonist ZM 241385 plus blocking anti-TIM3 mAb (Fig. 5H, I). In contrast, $CD4^+$ Treg infiltration was diminished (Fig. 5I). An enhanced ratio of $CD8^+$ CTL to $CD4^+$ Tregs in the tumor thus constitutes an additional potential mechanistic contribution of reduced tumor growth in mice upon blockade of the A2aR and TIM3.

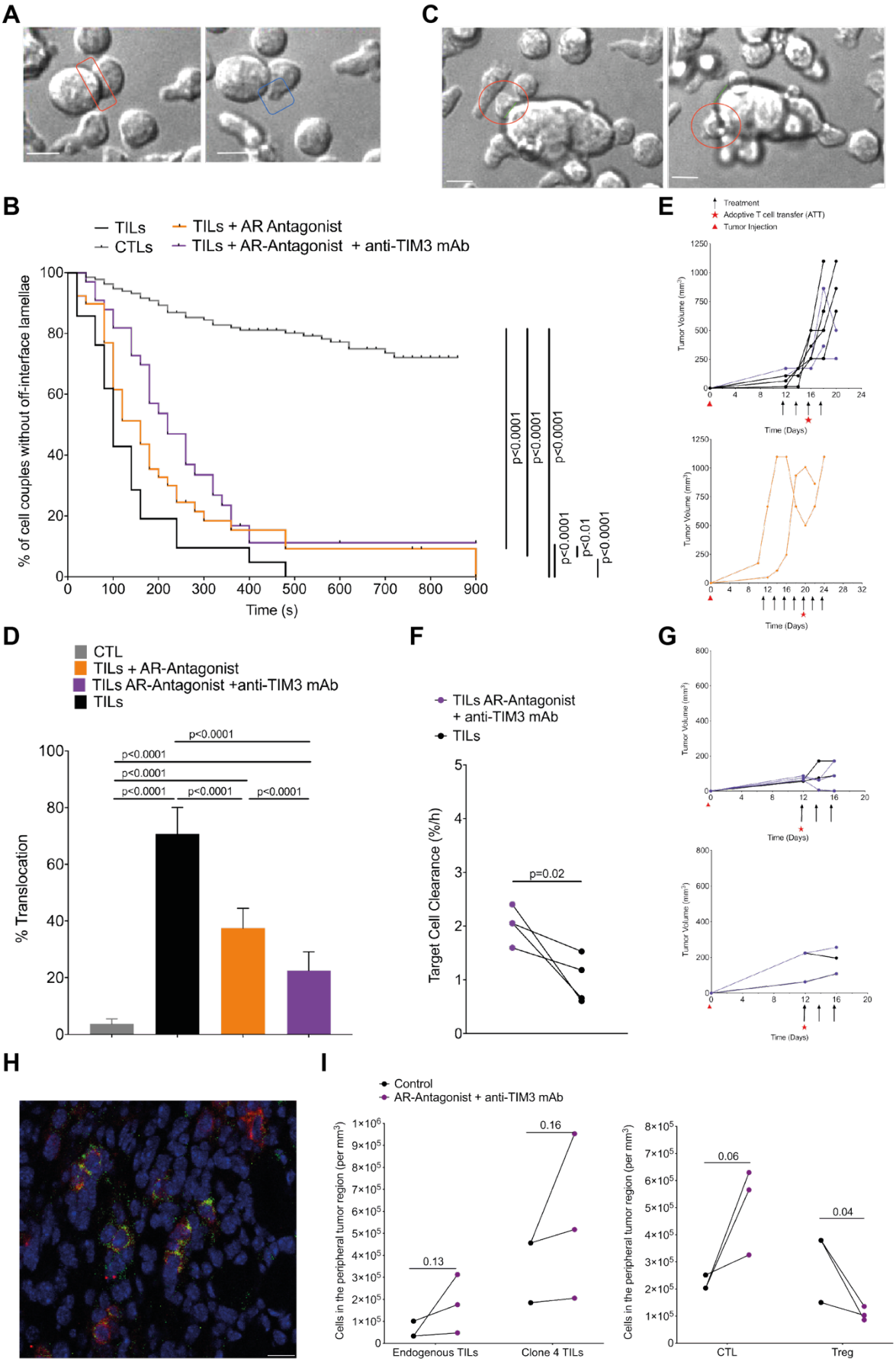

Figure 5 – A2aR plus TIM3 suppress CTL polarization, killing, and infiltration in the TME

A-E *Ex vivo* cytoskeletal polarization of CL4 TIL from RencaHA tumor-bearing BALB/c mice upon ATT of CL4 T cells and treatment with combinations of A2aR-Antagonist and anti-TIM3 mAb (N=5 control, N=3 both treatments, N=2 AR-Antagonist alone) in comparison to *in vitro* CL4 CTL is given. Mouse numbers across the different parts of the experiments are detailed in Fig. S2A. **A** Representative images of an off-interface lamella with the immune synapse in red and an off-interface lamella in blue. Scale bar=8µm. **B** Time until formation of the first off-interface lamella is given. Kaplan-Meier survival analysis (Log Rank) N>30 cell couples per condition over 4 experiments. **C** Translocation is shown as one CTL (red circle) moves >1 interface diameter from the initial location of the immune synapse (green) between early (left panel) and late (right panel) timepoints. Scale bar=8µm. **D** The frequency of cell couples with translocation is given. Pairwise proportion's z-test. N>30 cell couples per condition over 4 experiments. **E** Growth curves of the tumors used for analyses A-D are shown. **F** RencaHA tumor-bearing BALB/c mice were treated with A2aR antagonist and anti-TIM3 mAb from day 12. ATT of CL4 T cells was given on day 12. Killing of KdHA-pulsed Renca mCherry tumor cells by day 16 *ex vivo* CL4 TIL is given at an E:T ratio of 3:2. Each point=1 tumor, N=2 experiments. Size-matched tumors analyzed on the same day are paired for comparison using a t-test. **G** Growth of the tumors used for killing analysis in F are shown as two separate experiments. **H, I** Half of size-matched tumors from mice in E and G were stained. **H** A representative image with CD8 staining in red and Thy1.1 staining in green. scale bar=50µm. **I** The numbers of (left panel) endogenous $Thy1.2^+CD8^+$ TIL and adoptively transferred $Thy1.1^+$ Clone4 TIL or (right panel) total $CD8^+$ TIL and $FOXP3^+$ regulatory T cells in 10 peripheral and 10 central tumor areas are given. N=2 control tumors and 3 treated tumors analyzed over two experiments. Size matched tumors fixed on the same day are paired for analysis using t-test.

A2aR and TIM3 directly inhibit the killing of tumor target cells by CL4 CTL in spheroids

To determine whether A2aR and TIM3 directly regulate the interaction of suppressed CTL with their tumor target cells, we employed the *in vitro* reconstruction of CL4 CTL suppression in our Renca spheroid/CL4 CTL only system (Fig. 1). To determine roles of TIM3, we overexpressed a TIM3-GFP fusion protein in CL4 CTL. Such overexpression did not diminish spheroid infiltration by CL4 CTL (Fig. 6A). However, it diminished the ability of CL4 CTL to kill Renca target cells inside the spheroids as determined with DRAQ7 staining (Fig. 6B). Confirming TIM3-dependence, diminished Renca tumor cell killing could be reversed with the anti-TIM3 blocking mAb RMT3-23 (Fig. 6B). To determine roles of A2aR in tumor cell killing by CTL, we treated CL4 CTL/Renca spheroid co-cultures with the A2aR agonist CGS-21680 (31)(Fig. 6C-E). Such treatment led to a significant ($p<0.05$) reduction of CL4 CTL infiltration into the spheroids to about half of the level of infiltration seen with the vehicle only control (Fig. 6C, E), consistent with previously described enhancement of CTL infiltration into tumors upon A2aR antagonist treatment (21) and in A2aR-deficient mice (19). In CGS-21680 treated spheroids, Renca cell death was drastically diminished reaching only 16% of control at the 12h time point ($p<0.005$)(Fig. 6D, E). As the effect of CGS-21680 on killing is substantially greater than the effect on infiltration, reduced spheroid infiltration can only partially account for reduced tumor cell death upon treatment with the A2aR agonist. Therefore, A2aR likely also impairs the execution of tumor cell killing. In combination the spheroid data establish that A2aR and TIM3 directly suppress the ability of CL4 T cells to kill tumor target cells with an additional inhibitory effect of A2aR in reducing CTL infiltration.

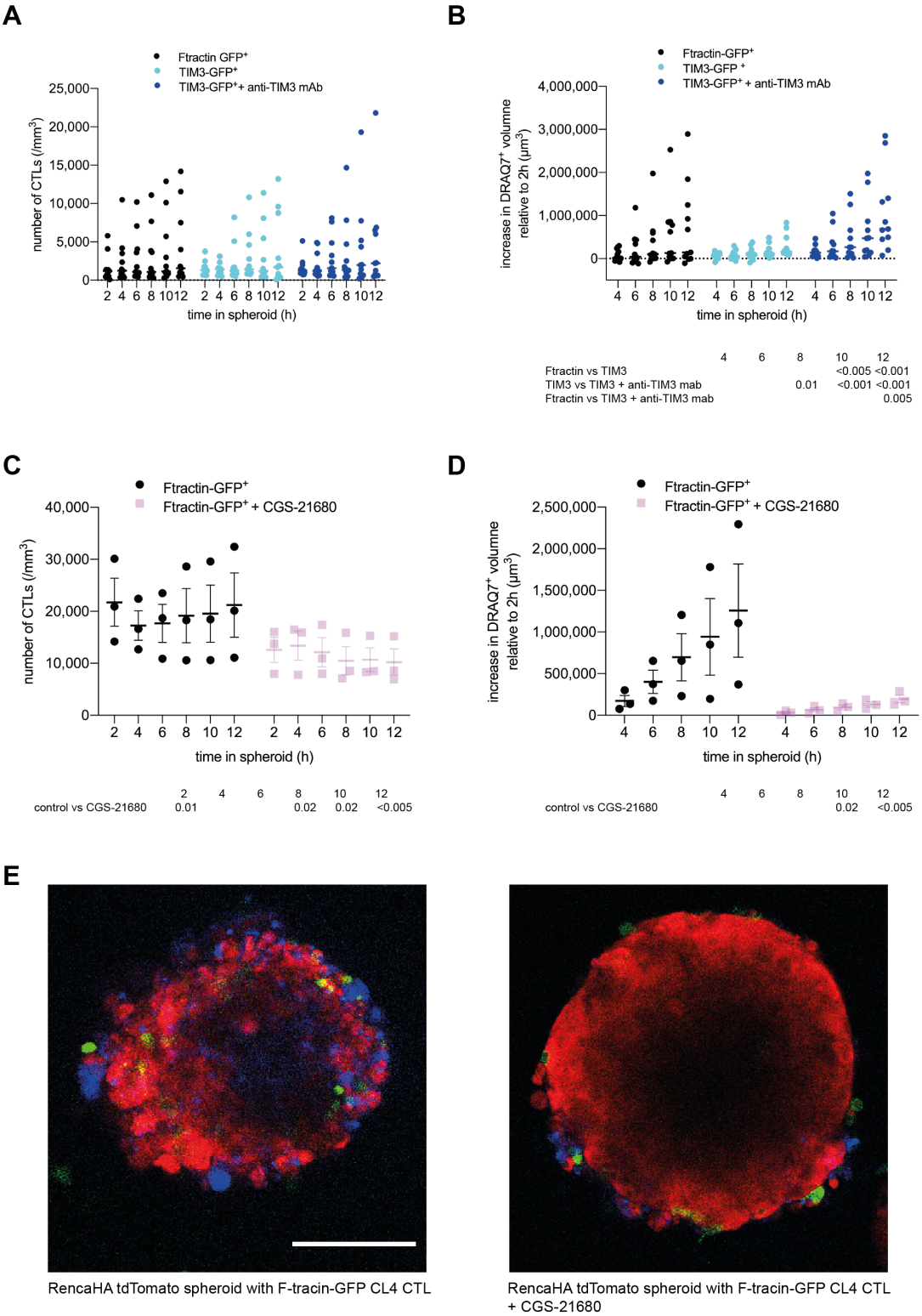

Figure 6 – A2aR and TIM3 suppress infiltration and killing of tumor spheroids by CTL

A, B CTL retrovirally transduced to express TIM3-GFP or F-tractin-GFP as a control were cocultured with RencaHA tdTomato spheroids incubated with K^dHA peptide for 12h ± 10µg/ml anti-TIM3 mAb (clone RMT3-23) with images acquired every 2h. Each data point is an independent experiment (n=11) with 5 or 6 spheroids analyzed per independent experiment. **A** SIL densities are shown as mean ± SEM. **B** Spheroid death, as measured by the increase in $DRAQ7^+$ spheroid volume, is shown for the same experiments as in A. **C, D** CL4 CTL transduced to

express F-tractin-GFP were co-cultured with RencaHA tdTomato spheroids ± 1µM CGS-21680. Each data point is an independent experiment (n=3) with 3 spheroids analyzed per independent experiment. **C** CL4 T cell densities are shown as mean ± SEM. **D** Spheroid death, as measured by the increase in DRAQ7$^+$ spheroid volume, is shown for the same experiments as in C. All data were analysed by 2-Way ANOVA, matched by independent repeat and timepoint. **E** Representative images of RencaHA tdTomato spheroids (red) with F-tractin-GFP-expressing CL4 CTL (green) as stained for cell death with DRAQ7 (blue) ± 1 µM CGS-21680 as indicated. scale bar=100µm with the same scale for both images.

Adenosine impairs CTL cytoskeletal polarization

Restoration of cytoskeletal polarization and increased tumor infiltration were mechanisms of immune enhancement *in vivo* in TIL from tumors treated with the A2aR antagonist ZM 241385 together with anti-TIM3 mAb. To determine direct roles of A2aR in cytoskeletal polarization and CTL effector function, we investigated CL4 CTL function *in vitro* (Fig. 1). Migratory T cells extend a leading lamella and form a uropod at the posterior end. CL4 CTL treatment with the A2aR agonist CGS-21680 reduced the percentage of CL4 T cells with a uropod from 80±4% in control-treated CL4 CTL to 25±5% ($p<0.001$)(Fig. 7A), indicative of suppression of the migratory phenotype. These data are consistent with the suppression of CL4 CTL spheroid infiltration upon treatment with CGS-21680 (Fig. 6C). Formation of a tight cell couple of a CTL with a tumor cell is the first step of killing and requires the effective extension of lamellae towards the target cell as a cytoskeletal polarization step. Upon treatment with CGS-21680 the frequency of CL4 CTL forming a tight cell couple upon contact with RencaHA target cells was significantly ($p<0.01$) reduced from 49±6% upon control treatment to 32±7% (Fig. 7B). In CTL tumor cell couples, T cell translocation over the tumor target cell surface and off-interface lamellae are defining cytoskeletal features of suppressed TIL. Treatment of CL4 CTL with 1µM or 10 µM of the pan-adenosine receptor agonist NECA enhanced the percentage of CL4 CTL that translocated over the tumor target cell surface from 4±2% to 36±9% and 29±4%, respectively ($p<0.001$)(Fig. 7C). This enhancement was reversed by parallel treatment with the A2aR antagonist ZM 241385, establishing that it was predominantly mediated by A2aR. Similarly, off-interface lamellae became more frequent upon CL4 CTL treatment with NECA and formed more rapidly, as both partially reversed by parallel treatment with ZM 241385 (Fig. 7D). Together these data establish that engagement of A2aR on CTL suppresses cytoskeletal polarization at multiple stages of CTL function, migration, cell couple formation and the maintenance of a fully polarized cell couple. These data corroborate a cytoskeletal mechanism for A2aR-mediated suppression of TIL function. They also constitute an interesting contrast to PD-1, as investigated in the same experimental system (7). As CTL constitutively express PD-1 and Renca cells PD-L1, we used anti-PD-1 to investigate the role of PD-1 in cytoskeletal polarization. Rather than restoring CL4 CTL and *ex vivo* TIL cytoskeletal polarization as expected for blocking an inhibitory interaction, anti-PD-1 increased the frequency of occurrence of off-interface lamellae and the translocation phenotype (7). In addition, calcium signaling was impaired not enhanced (7). The inhibition of cytoskeletal polarization in the direct interaction of CTL with their target cells by A2aR thus is in contrast to the stimulatory role of PD-1.

Cytoskeletal polarization also contributes to CTL signaling and effector function other than migration and killing. We therefore investigated CTL calcium signaling and naïve T cell proliferation. The elevation of the cytoplasmic calcium concentration in CL4 CTL upon interaction with K^dHA peptide-pulsed Renca tumor target cells was partially inhibited by

treatment with CGS-21680 (Fig. 7E). Proliferation of naïve CL4 T cells upon stimulation with anti-CD3/CD28 was partially inhibited by 1µM or 20µM NECA, as reversed with parallel treatment with the A2aR antagonist ZM 241385 without reaching statistical significance (Fig. 7F). An only moderate effect of A2aR on T cell proliferation has been previously reported (17). A determination of whether these defects are secondary to impaired cytoskeletal polarization or independent thereof is beyond the scope of this manuscript. Such defects, albeit moderate in size, may contribute to the immune-suppressive function of A2aR.

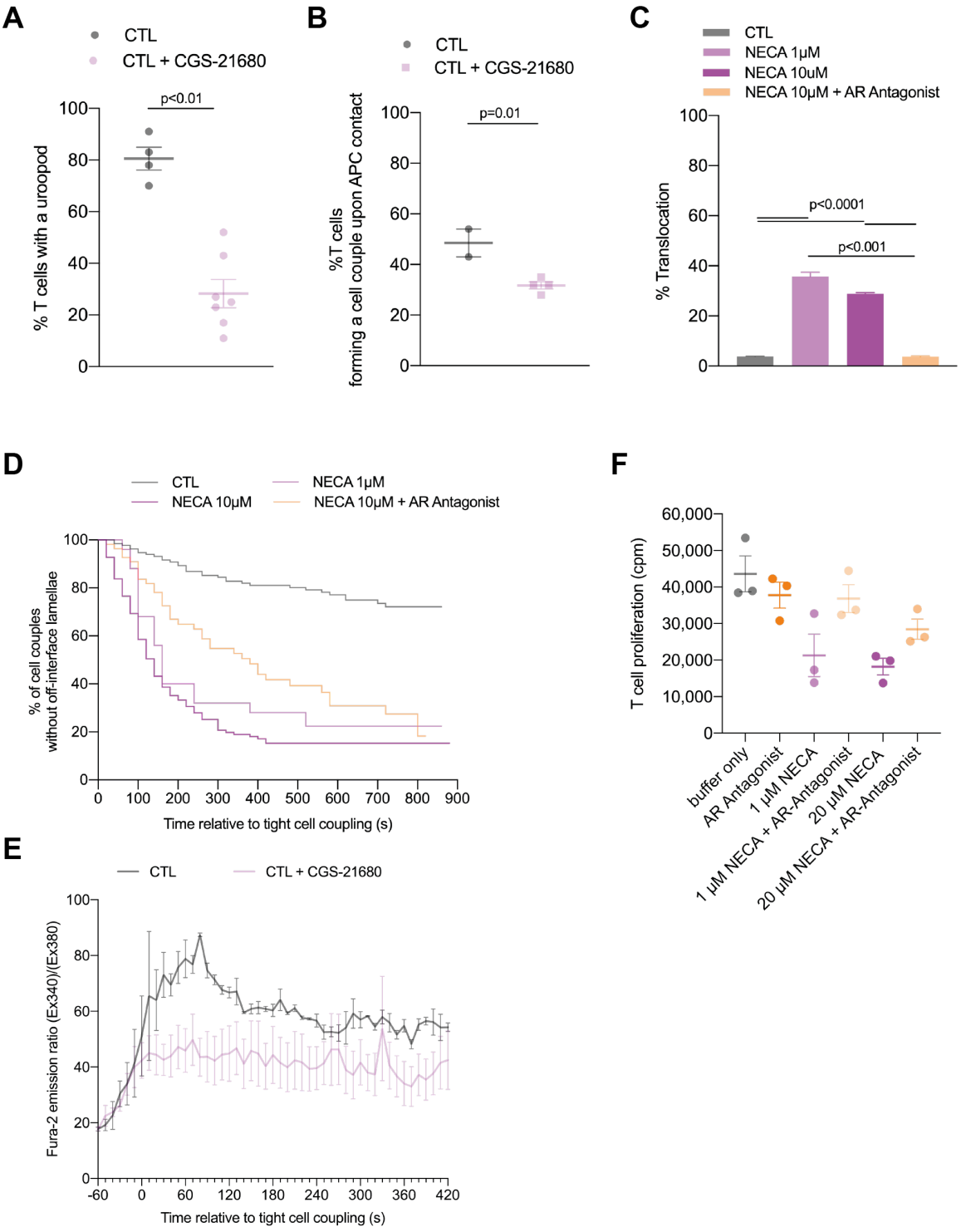

Figure 7 – A2aR suppresses the cytoskeletal polarization of CTL

A Percentage of *in vitro* CL4 CTL with a uropod ± 1µM CGS-21680. N=4 independent experiments, 220/648 T cells analyzed. **B** Frequency of CL4 T cells that form a tight cell couple upon contact with a Renca APC incubated with 2µg/ml K^dHA peptide. N=2 independent experiments, 68/234 T cells analyzed. **C, D** Imaging of the interaction between *in vitro* CL4 CTL with KdHA-pulsed Renca tumor cell targets treated with NECA ± 1.25 µM A2aR-Antagonist. **C** Percentage of cell couples with translocation (pairwise proportion's z-test). N>30 cell couples per condition over 2-4 experiments. **D** Time until formation of first off-interface lamella (Kaplein-Mayer

survival analysis (Log Rank)). P<0.01 all comparisons. **E** *In vitro* CL4 CTL interacted with RencaHA cells incubated with 2µg/ml K^dHA peptide ± 1µM CGS-21680. The ratio of Fura-2 emissions at 510nm upon excitation at 340nm over 380nm is given relative to time of tight cell coupling. N=2 independent experiments, 13/42 T cells analyzed. **F** CL4 T cells were primed *in vitro* using anti-CD3/CD28 mAb. NECA ±1.25µM ZM 241385 were added at 0h and ^{3}H-thymidine for the last 8h of cell culture. Proliferation was quantified by ^{3}H-thymidine incorporation (cpm) (N=3 experiments).

Discussion

To build a diverse tool kit of reagents for comprehensive cancer immunotherapy, it is vital we understand mechanisms of action of mediators of immune suppression. Using a matched *in vivo*, *ex vivo* and *in vitro* spheroid approach, we have established that A2aR and TIM3 directly suppress the ability of CTL to kill tumor target cells. The focus on a direct effect of checkpoint blockade regimens on CTL responses is important as a complement to current inhibitory receptor blockade therapies. CTLA-4 and PD-1 blockade improve the anti-tumour immune response amongst patients with melanoma, NSCLC and haematological cancers (11, 32), however, frequently with significant adverse immunological effects. PD-1 and CTLA-4 are expressed during T cell differentiation and by CTL throughout the body. Moreover, they are expressed by other cell types, such as myeloid cells and regulatory T cells, respectively. Action on myeloid cell types and the generation of new T cell clones at priming, potentially including autoreactive ones, may be a principal mechanism of PD-1 and CTLA-4 blockade with only secondary effects on CTL killing (33, 34): In basal and squamous cell carcinoma patients, anti-PD-1 does not lead to the activation of existing anti-tumor T cell clones but to tumor enrichment of new ones (6). In a mouse melanoma model deletion of PD-1 in T cells does not enhance anti-tumor immunity; however, deletion of PD-1 in myeloid cells does (5). We showed that blocking PD-1 in the *in vitro* interaction between CTL and tumor cells actually impaired, rather than improved, killing and the necessary cytoskeletal polarization steps (7). The direct role of A2aR and TIM3 in regulating CTL – tumor cell interaction thus generates a promising contrast to PD-1 and CTLA-4, as already investigated in early stage clinical trials (24, 35).

Despite such promise, it is still unclear whether or not blocking A2aR and/or TIM3 will lead to fewer autoimmune side effects. Adenosine, A2aR and TIM3 not only suppress T cell function but also that of myeloid cells (36, 37). However, effects of adenosine in myeloid cells may be mediated by another adenosine receptor, A2bR (38). A2aR expression in T cells also contributes to thymic development and in the maintenance of a quiescent state among naïve T cells (39). Autoimmunity upon melanoma rejection in A2aR-deficieny mice has been observed (17). Nevertheless, approval of the A2aR antagonist Istradefylline for the treatment of Parkinson's Disease (40) and several early phase clinical trials of the A2aR antagonist CPI-444 in cancer indicate that autoimmune side effects of A2aR blockade can be minimal.

CTLA-4 and PD-1 have greatest efficacy in tumors that possess large numbers of infiltrated $CD8^+$ TIL, which are predominantly suppressed by inhibitory receptor expression (11). However, such 'hot' tumors represent only a minority of all cancer types, prominently melanomas. In contrast, cold tumors lack an immune infiltrate almost entirely. In altered immunosuppressed and altered-excluded tumors cancer-specific CTL priming and infiltration do occur but tumor-mediated immune suppression, rather than relying predominantly on inhibitory receptors, employs alternate suppressors such as adenosine and prostaglandin E2, Tregs, and inhibitory cytokines such as IL-10 and TGF-β (11). Moreover, infiltration of CTL into tumors can often be partial, reaching only the peripheral stromal regions of the tumor mass. Therapeutic approaches to increase tumor infiltration by CTL are therefore important in extending immunotherapy to cold and altered phenotype cancers. CTL tumor infiltration is enhanced in A2aR-deficient mice, mice with selective A2aR deletion in T cells and upon A2aR agonist treatment, albeit in experiments using hot mouse tumor models (19-21). In a various

mouse models CD73 activity on non-hematopoietic cells limited tumor infiltration of T cells (41). Increased tumor infiltration of $CD8^+$ CTL upon A2aR blockade may occur because A2aR regulates the endothelium (42). In addition, CTL-intrinsic mechanisms of enhanced tumor infiltration are likely. We showed that A2aR engagement could efficiently block CL4 CTL infiltration of spheroids (Fig. 6C). A2aR engagement directly suppresses $CD8^+$ T cell migration through inhibition of the KCa3.1 ion channel (43). Adenosine may also regulate the infiltration of other in immune cell types, as blockade of CD73 leads to increased dendritic cell infiltration in the context of radiotherapy of poorly immunogenic tumors (37).

Blockade of A2aR led to compensatory upregulation of inhibitory receptor expression as previously noted (13, 44). Compensation between different elements of tumor-mediated immune suppression has been described before, e.g. in the upregulation of A2aR expression upon PD-1 blockade (45). Curiously, blocking A2aR during vaccination leads to diminished inhibitory receptor expression on T cells (18). In a model of colon cancer, A2aR blockade doesn't alter PD-1 expression on $CD8^+$ TIL but reduced it on T cells in the tumor-draining lymph nodes (18). Effects of A2aR blockade on inhibitory receptor expression thus may be context-dependent.

A key mechanism of A2aR and TIM3 in regulating CTL function is the suppression of cytoskeletal polarization in T cell migration and target cell killing. We can only speculate on underlying signaling mechanisms. A2aR signaling through cAMP/protein kinase A results in inhibition of RhoA and Cdc42 in leukocytes during cell-cell adhesion (46). In cardiomyocytes, adenosine receptor agonists prevent RhoA activation and cofilin-mediated actin polymerization (47). In addition, A2aR and TIM3 could converge on the tyrosine kinase Lck. Elevated cAMP levels in response to A2aR engagement can enhance Csk activity (13, 48), leading to inhibitory phosphorylation of Lck. When not engaged by ligand, TIM3 binds BAT3, a molecule which maintains a reservoir of Lck at the immune synapse and thus lowers the threshold for TCR signaling. TIM3 binding to Galectin-9 or Ceacam-1 releases BAT3, disabling Lck pre-localization at the immunological synapse (49).

In summary, our work supports blocking of A2aR and TIM3 as an attractive complement to PD-1 and CTLA-4 blockade in anti-tumor immunotherapy. A2aR and TIM3 blockade directly enhanced the ability of CTL to polarize towards and kill tumor target cells in tumors and tumor spheroids and may thus reactivate tumor-resident suppressed CTL. In addition, regulation of tumor and spheroid infiltration by A2aR promises therapeutic potential in cold and altered immunity tumors.

Materials and Methods

Mice

Thy1.2$^{+/+}$ BALB/c, (Charles River, Oxford, UK) and Thy1.1$^{+/+}$ CL4 TCR-transgenic mice [Research Resource Identifier (RRID): IMSR_JAX:005307] were maintained at the University of Bristol Animal Services Unit. All mouse experiments were compliant with UK Home Office Guidelines under PPL 30/3024 to DJM.

Antibodies

Antibodies used are described in the order: antigen, fluorescent label, clone, supplier, dilution:

For flow cytometry:

FcBlock no azide (for blockade of Fc receptors) 2.4G2 BD Biosciences 1:50
CD8α FITC 53-6.7 BD Bioscience 1:100
CD8β PeCy7 YTS156.7.7 Biolegend 1:200
CD4 AF700 CKI1.5 Biolegend 1:100
CD39 PerCP-Cy5.5 24DMSI eBioscience 1:100
CD73 BV605 T111.8 Biolegend 1:100
TIM3 PE B8.2C1.2 Biolegend 1:100
TIM3 BV605 RMT3-23 Biolegend 1:100
TIGIT APC 1G9 Biolegend 1:100
LAG3 PeCy7 C9B7W eBioscience 1:200
PD1 BV785 29F.1A12 Biolegend 1:200
TCRβ AF647 H57-597 Biolegend 1:200
Thy1.1 FITC OX7 BD Bioscience 1:100
Thy1.1 PerCP-Cy5.5 OX7 Biolegend 1:100
CEACAM1 APC CC1 Biolegend 1:100

For blocking and T cell priming

TIM3 no azide (for *in vitro/in vivo* blockade) RMT3-23 BioXcell In Vivo mAb *in vivo:* 100µg/mouse in vitro: 10µg/ml
Isotype control for anti-TIM3 Rat IgG2a 2A3 no azide (for *in vivo/in vitro* blockade) BioXcell In Vivo mAb *in vivo:* 100µg/mouse *in vitro:* 10µg/ml
CD8β no azide (for *in vivo* depletion) 53-5.8 BioXcell InVivoMAb 100µg/mouse
Thy1.1 no azide (for *in vivo* depletion) 19E12 BioXcell InVivoMAb 250µg/mouse
CD3ε no azide (for *in vitro* priming) 145-2C11 BioXcell InVivoMAb 10µg/ml
CD28 no azide (for *in vitro* priming) 37.51 BioXcell InVivoMAb 1µg/ml

For immunohistochemistry:

FcBlock no azide (for blockade of Fc receptors) 2.4G2 BD Biosciences 1:50
CD8α no azide 53-6.7 Biolegend 1:500
Rabbit H+L AF488 Life Technologies 1:1000
Rabbit H+L AF405 Life Technologies 1:1000
Rat IgG2a,κ Biolegend 1:500
Rat IgG H+L AF594 ThermoFisher 1:2000

FOXP3 no azide FJK-16S ThermoFisher 1:100
FOXP3 APC FJK-16S ThermoFisher 1:40
Thy1.1 FITC OX7 BD Bioscience 1:100
Isotype control for Thy1.1 Mouse IgG1,κ FITC BD Bioscience 1:100
CD19 (dump) BV510 6D5 Biolegend 1:100
TCRβ SB645 H57-597 ThermoFisher 1:200
CD4 PE-Cy5.5 RM4-5 ThermoFisher 1:3000
CD8β PE-Cy5 H35-17.2 ThermoFisher 1:3000
CD25 VioBright-FITC 7D4 Miltenyi 1:200
CD73 BV605 TY/11.8 Biolegend 1:100
CD39 PerCP-eFluor710 24DMS1 ThermoFisher 1:100

Cell culture

Murine Renal Carcinoma cell lines and Phoenix retrovirus-producing cell lines were maintained as previously described (7).

To generate *in vitro* CL4 CTL, CL4 mouse spleens were macerated. Red blood cells were lysed using ACK Lysis buffer (Gibco, ThermoFisher, Gloucester UK), and the remaining splenocytes were resuspended in complete medium, RPMI-1640 with 10% FBS and 50μM 2-mercaptoethanol. $5x10^6$ cells were seeded into each flat bottomed 24 well tissue culture plate with 1μg/ml of K^dHA peptide ($IYSTVASSL_{[518-526]}$) from influenza virus A/PR/8/H1N1, for 24 hours at 37°C. After 24h, cells were washed 5 times in RPMI (Gibco) and reseeded in to 24 well pates at $5x10^6$ cells per well in 2ml complete medium containing 50 units/ml of recombinant human IL-2 (National Institutes of Health/NCI BRB Preclinical Repository). Retroviral transduction was performed if required as previously described (7). CL4 T cells were then passaged every 12 to 24 hours using fresh IL-2 containing complete medium. Where indicated, NECA (Sigma), ZM 241385 (Santa Cruz) or CGS-21680 (Tocris) were added to cell culture. DMSO was used as vehicle control.

For ^{3}H-thymidine proliferation assays (50), Clone 4 T cells were primed using anti-CD3/CD28 mAb stimulation or with mature agonist-peptide pulsed dendritic cells in a flat bottomed 96 well plate and cultured for the desired time at 37°C. ^{3}H-thymidine (Amersham Life Science, London, UK) was added for the final 8h of cell culture at 1.45mBq/ml. To harvest, the entire plate was frozen at -20°C for at least 24 hours and subsequently defrosted to produce cell lysis. ^{3}H-thymidine incorporation was measured using a 96 well Tomtec harvester and a Microbeta scintillation counter (PerkinElmer).

Extraction of T cells from tumor tissue was carried out using magnetic activated cell sorting (Miltenyi) and flow cytometry as described in (7).

Tumor Growth and Treatment Experiments

6-week-old $Thy1.2^{+/+}$ BALB/c mice were injected subcutaneously, in the dorsal neck region, with $1x10^6$ RencaHA tumor cells in 100μl PBS. Tumor measurements and treatment commenced at day 12, when tumors of approximately 5 x 5mm diameter were palpable. For adoptive transfer experiments, tumor-bearing mice were injected i.v. at day 12, with $5x10^6$ day 5 CL4 CTL (see above). For *in vivo* immunotherapy, control mice received 100μl vehicle (15% vol/vol DMSO, 15% vol/vol Cremophore EL, 70% vol/vol PBS) +/- 100μg/mouse isotype control (Rat IgG2a, 2A3, BioXcell InVivoMAb)(51). Treated mice received combinations of 10mg/kg ZM 241385 injected intraperitoneally in 100μl vehicle and 100μg/mouse anti-TIM3

mAb (RMT3-23, BioXcell InVivoMAb) injected intraperitoneally in 100µl PBS on alternate days throughout the experiment. Tumors were measured on alternate days using calipers and the volume calculated using the modified elliptical formula: Volume = 0.5 x length x width^2. CL4 CTL restimulation *in vivo* was achieved by i.p injection of 200µl of PBS containing 1200 HA units of influenza virus A/PR/8/H1N1 virus, as in (27). Rechallenge with tumor cells was achieved following stable remission (remained <5 mm diameter for 8 days) by injecting a further 1x10^6 RencaHA cells subcutaneously into the dorsal neck region in PBS. Depletion of CD8$^+$ or Thy1.1$^+$ T cells was performed by injection of depleting mAb (anti-CD8, 53-5.8, BioXcell InVivoMAb, 100µg/mouse, Thy1.1 19E12 BioXcell InVivoMAb, 250µg/mouse).

Imaging and Image Analysis

For live cell imaging of immune synapse formation and CL4 T cell morphology 1x10^6 Renca tumor target cells were pulsed with 2µg/ml K^{d}HA for 1 hour at 37°C. Cells were then resuspended at 1x10^6/400µl Imaging Buffer (PBS, 10% FBS, 1mM $CaCl_2$, 0.5mM $MgCl_2$). To image the increase in the cytoplasmic Ca^{2+} concentration, CL4 CTL were incubated with 2µM Fura-2 AM (Molecular Probes) for 30min at room temperature in imaging buffer and washed twice thereafter.

40,000 Clone 4 CTL or TIL in 5µl imaging buffer were plated with 1- 1.5µl Renca target cells (preceding paragraph) in 50µl imaging buffer, in a 384-well, glass-bottomed imaging plate (Brooks). If reagents such as NECA were included in cell culture, they were also added to imaging buffer at an equivalent final assay concentration. Every 10s for 15min, one bright-field differential interference contrast (DIC) image, one fluorescence image with excitation at 340 nm, and one fluorescence image with excitation at 380nm were acquired at 37°C with a 40x oil objective (NA = 1.25) on a Leica DM IRBE-based wide-field system equipped with Sutter DG5 illumination and a Photometrics Coolsnap HQ2 camera.

Using MetaMorph (Molecular Devices) for analysis of DIC images, tight cell couple formation was defined as the first time point at which a maximally spread immune synapse formed, or two frames after initial cell contact, whichever occurred first. To assess CTL and TIL morphology, every DIC frame after tight cell couple formation was assessed for the presence of off-synapse lamellae, defined as transient membrane protrusions pointing away from the immune synapse, followed by retraction. To determine CTL translocation over the Renca cell surface, the position of the immune synapse on the RencaHA target cell was compared to the position at cell coupling. If the T cell had migrated by a distance greater than the diameter of the immune synapse, this was classed as translocation. For calcium analysis, field-averaged background fluorescence was subtracted from the 340nm and 380nm excitation fluorescence data, and the ratio of the Fura-2 images upon excitation at 340 versus 380 nm was determined in a circular region of interest of the dimensions of the T cell.

For Microscope-based Cytotoxicity Assays, the IncuCyte™ Live Cell analysis system and IncuCyte™ ZOOM software (Essen Bioscience) were used to quantify target cell death. 1x10^6 Renca cells transfected to express the fluorescent protein mCherry were either untreated (control) or pulsed with 2µg/ml K^{d}HA peptide for 1 hour. Cells were centrifuged and resuspended in 3.33ml Fluorobrite complete medium (Thermo Fisher) to a concentration of 15,000 cells/50µl. Cells were plated in each well of a 384 well Perkin-Elmer plastic-bottomed view plate and incubated for 4 hours to adhere. CL4 T cells were FACS sorted and 15,000 cells

added to the plate in 50µl Fluorobrite medium 4 hours after target cells were plated, yielding an 1:1 effector to target ratio. Images were taken every 15 minutes for 14 hours at 1600ms exposure using a 10x lens. The total red object (mCherry target cell) area (µm^2/well) was quantified at each time point. The T cell killing rate was determined as the linear gradient of the red object data at its steepest part between the time at which Control Clone 4 CTL started killing, until they had eradicated the Renca cell monolayer. The T cell killing rate was normalized to the growth of Renca (control) cells which were not pulsed with cognate HA antigen.

Spheroids

RencaHA tdTomato cells were resuspended at a concentration of 1×10^5 cells/ml, mixed with Matrigel (Corning) at 4°C, seeded in a 24-well plate at a final concentration of 500 cells per Matrigel dome, and left to solidify for 10min at 37°C. 2ml cell medium was added to each well and cells incubated at 37°C for 11 days. Each Matrigel dome was washed twice in PBS and incubated for 30min with 1ml of Cell Recovery Solution (Corning). Spheroids were collected in a 15-ml Falcon tube and pulsed with K^{d}HA peptide at a final concentration of 2µg/ml for 1 hour. Pulsed spheroids were re-embedded in Matrigel together with 5×10^5 primed CL4 CTL per Matrigel dome. Matrigel domes were dissolved for analysis of spheroid-infiltrating T cells after 16h: Spheroids were washed twice in PBS and incubated with 1ml of Cell Recovery Solution (Corning). Spheroids were collected, washed through a 70µm sieve and then disaggregated to retrieve T cells in 500µl of imaging buffer for immediate FACS sorting.

Spheroid imaging

Spheroids were grown as described in the preceding paragraph. On day 10, CL4 CTL that had been retrovirally transduced to express the GFP-tagged protein of interest (TIM3-GFP or F-tractin-GFP) were sorted by flow cytometry and incubated in IL-2 medium for 1h ± 10µg/ml anti-TIM3 mAb (Clone RMT3-23) or 1µM CGS-21680 where appropriate. Meanwhile, spheroids were dissociated from Matrigel and resuspended into fresh Matrigel at a concentration of ~8 spheroids/µl. 50µl of the spheroid-Matrigel suspension was separated into Eppendorf tubes for each treatment group, followed by the addition of 200,000 sorted T-cells per tube. 50µl of Matrigel, containing spheroids and T cells, was plated into each well of a 24-well tissue culture plate. After Matrigel had set, 1ml of Fluorobrite medium was added to each well, containing 1.5µM DRAQ7 viability dye ± 10µg/ml anti-TIM3 mAb or 1µM CGS-21680. Images were acquired every 2h post-plating CTL with spheroids in 3µm z steps from the bottom of the spheroid to its widest point, usually 40 steps, for 12h using a Leica SP8 AOBS confocal microscope with a 10x HC PL Fluotar lens (NA=0.3). To obtain measurements of SIL density and spheroid dead volumes, raw data was pre-processed and semi-automatically analysed using a custom-written Cancer Segmentation workflow for the Fiji (52) plugin, MIA (v0.9.26) and its MIA_MATLAB (v1.1.1) package, available at Github via Zenodo: http://doi.org/10.5281/zenodo.2656513 and http://doi.org/10.5281/zenodo.4769615, respectively. Briefly, the imaged stacks were mirrored and concatenated along the z-axis to produce pseudo-complete spheroids. These spheroids were binarised and segmented using connected-components labelling (53). To account for fragmented spheroid segmentation arising from gaps in labelling, in particular towards spheroid centers, spheroids were fit with alpha shapes (54) using the MATLAB implementation. Adjacent spheroids which had become merged during processing were separated with a distance-based watershed transform (53). T-cells and dead volumes were individually segmented from their respective fluorescence

channels using similar threshold and labelling-based processes, albeit without the alpha shape step.

Flow cytometry staining

MACS-purified TIL were resuspended in PBS at a concentration of $1x10^6$ cells/ml. $2.5x10^5$-$1x10^6$ cells for each condition resuspended in 100µl PBS per tube with 1µl/100 µl Zombie Aqua Fixable Live Cell Detection reagent (Biolegend). Tubes were incubated for 15 minutes in the dark at room temperature. Cells were washed in 3ml FACS buffer and resuspended in 100µl per tube FcBlock (BDBiosciences) for 15 minutes at 4°C. Cells were washed in 3ml FACS buffer, pelleted and resuspended in 100µl FACS buffer per tube with antibody at the required concentration (antibody section above) and then incubated for 30min at 4°C. Antibody concentration was determined by titration using 5 concentrations centered around the manufacturer's recommended protocol. Cells were washed in 3ml FACS buffer before being fixed in 1% paraformaldehyde and analyzed within 5 days using a Fortessa Flow Cytometer and BD FACSDiva Software (BD Biosciences). Flow cytometric data were analyzed using FlowJo™ (Treestar) software. Gating was performed using fluorescence minus one (FMO) samples for each antibody stain.

Immunohistochemistry

Tumors were harvested and cut in half. Half of the tumor was used for CTL function assays. The other half was placed in 2.35ml RPMI on ice. Within 1 hour of harvest, tumors were snap-frozen in OCT compound (Tissue Tek) on a square of cork in an isopentane bath, hovering above Liquid Nitrogen. Tumors were sectioned into 5µm sections and mounted on slides. On day one of staining, acetone was cooled to -20°C. Slides were allowed to air dry for 10–20min before being fixed in acetone for 10min on ice. Slides were dried again then washed three times in PBS. Slides were dried in the area around the section and a border marked using a hydrophobic pen (ImmEdge). Sections were blocked with 2.5% horse serum (Vector) for 30min then washed three times in PBS. Sections were incubated with primary antibodies or isotype controls in 1% BSA/PBS (Sigma-Aldrich) overnight at 4°C or room temperature for 1h (antibody section above). On day 2 of staining, slides were washed three times with PBS and incubated with secondary antibody prepared in 1% BSA/PBS for 30-60min at room temperature (antibody section above). Slides were washed three times in PBS, with the second wash being performed in a shaker for 10 minutes. Hoechst stain (Thermofisher) was applied for 10min, followed by three PBS washes. Slides were fixed in 1% PFA for 10 min then washed twice in PBS, once in Glycine (0.3M)(Fisher Chemical) for 10 min and 1 final wash in PBS. Coverslips were mounted in prolong gold antifade reagent and slides were left to cure at room temperature for 24 hours and images were acquired using a mark and find experiment on the same confocal microscope as used for spheroid imaging. Images were analyzed using ImageJ (Fiji).

Data Analysis and Statistics

The Power of *in vivo* experiments was designed to reach >80%. Experimental group size was determined using the equation: $n = (2/(\text{standardized difference}2)) \times cp,power$, where n = sample size per group determined using the formula, d = standardized difference = measurable difference in tumor volume / standard deviation, cp,power = constant for $p<0.01$ and power at 80% defined using standard Altman's Nomogram = 11.7.

Samples were compared using independent sample t-tests for two sample comparisons. To determine the effect of one or more independent variables on one dependent variable across >2 groups, One way and Two-way ANOVA were used. Where proportions were compared, Fisher's exact Boschloo or a proportion's z-test was used. SPSS statistics and Prism were used to execute analyses.

In analyses of *in vivo* tumor growth and survival, the following factors were considered:

1. *Experiments using Single Agent treatment of RencaHA tumors* When single immunotherapy was administered, tumor growth was unidirectional and tumors did not shrink, therefore repeated measures ANOVA was utilized to compare growth curves. Kaplan–Meier analysis was used to compare survival (Mantel Cox, Log rank), since there were only two outcomes in the study, survival or death. Mice were censored if tumors were < maximal allowable tumor size (MATS) or if culled for reasons other than tumor size (such as ulceration). Mice bearing tumors > MATS were culled and recorded as dead.
2. *Experiments using combined treatment with Adoptive T cell transfer, TIM3 blockade and A2aR blockade:* Cohorts of 14 mice per group were injected to achieve minimum 4-6 tumors per group of uniform size (3-5 mm diameter) between 12-14 days after injection, for each experimental replicate. Tumor growth was compared using R values. To account for growth over the whole triphasic growth curve, final volume/initial volume is used because an exponential model cannot be applied to tumor growth greater than 1 week (55-57). For early stage tumors, an exponential model was fitted. R value (units of R = 1/time) was calculated using: R = c(dc/dt) where: qg = 2.76×10^5 Renca tumor cell = 17-25 µM diameter in vitro = 3.61 nm^3 volume using modified elliptical formula. Therefore 2.76×10^5 Renca cells make up 1 mm^3 of tumor. Each Renca cell divides 3 times every 24 hours, dt =8h, dc = difference in cell number = (qg x final volume in mm^3) – (qg x starting volume in mm^3), c = number of cells at start = (qg x starting volume in mm^3) (55-57). Progression free survival was calculated using Cox's regression with covariates (SPSS). Hazard ratio of relapse was calculated using SPSS statistics.

Analysis of Flow Cytometric Data: Flow cytometric data were analyzed using FlowJo™ (Treestar). Gating was performed using Fluorescence Minus One control samples. Boolean gating tool was used to determine all possible combinations of expression of certain markers. Percentage expression of co-inhibitory receptors as determined by flow cytometry were arcsine square root transformed prior to analysis. Tumor volume was $\log_{10}$ transformed. Principal component analysis (PCA) was performed using RStudio™ to analyze the combination expression of 6 markers as determined by flow cytometry, and tumor volume. Tumors with a growth rate >1 standard deviation from the mean were excluded from comparisons. After transformation, each value (x) within the expression data and volume data were standardized (x*) to give a mean (m) of 0 and a standard deviation (SD) of 1 using the formula x* = (x-m)/sd. PCA was then performed using R studio and the packages '*FactoMineR'* and *'Factoextra'*. Principal components (PC) 1-5 were selected for inclusion based on eigenvalues >1. Cos2 values were used to confirm the quality of representation of each variable within 2-dimensional factor maps and were calculated as the square of the variable's co-ordinates. The contribution of variables to PCs 1-4 was calculated using the formula (var.cos2 * 100) / (total cos2 PC) to produce P values.

Data availability

Two large data sets, the flow cytometry data underpinning the principal component analysis to determine inhibitory receptor expression upon A2aR blockade and the spheroid imaging data, are accessible at https://data.bris.ac.uk/data/ under DOI tbd. All other data will be made available upon request.

References

1. Hegde PS, Chen DS. Top 10 Challenges in Cancer Immunotherapy. Immunity. 2020;52(1):17-35.
2. Schildberg FA, Klein SR, Freeman GJ, Sharpe AH. Coinhibitory Pathways in the B7-CD28 Ligand-Receptor Family. Immunity. 2016;44(5):955-72.
3. Anderson AC, Joller N, Kuchroo VK. Lag-3, Tim-3, and TIGIT: Co-inhibitory Receptors with Specialized Functions in Immune Regulation. Immunity. 2016;44(5):989-1004.
4. Wolchok JD, Kluger H, Callahan MK, Postow MA, Rizvi NA, Lesokhin AM, et al. Nivolumab plus ipilimumab in advanced melanoma. The New England journal of medicine. 2013;369(2):122-33.
5. Strauss L, Mahmoud MAA, Weaver JD, Tijaro-Ovalle NM, Christofides A, Wang Q, et al. Targeted deletion of PD-1 in myeloid cells induces antitumor immunity. Sci Immunol. 2020;5(43).
6. Yost KE, Satpathy AT, Wells DK, Qi Y, Wang C, Kageyama R, et al. Clonal replacement of tumor-specific T cells following PD-1 blockade. Nat Med. 2019;25(8):1251-9.
7. Ambler R, Edmunds GL, Tan SL, Cirillo S, Pernes JI, Ruan X, et al. PD-1 suppresses the maintenance of cell couples between cytotoxic T cells and target tumor cells within the tumor. Sci Signal. 2020;13(649):eaau4518.
8. Sharma A, Subudhi SK, Blando J, Scutti J, Vence L, Wargo J, et al. Anti-CTLA-4 Immunotherapy Does Not Deplete FOXP3(+) Regulatory T Cells (Tregs) in Human Cancers. Clin Cancer Res. 2019;25(4):1233-8.
9. Sharma A, Subudhi SK, Blando J, Vence L, Wargo J, Allison JP, et al. Anti-CTLA-4 Immunotherapy Does Not Deplete FOXP3(+) Regulatory T Cells (Tregs) in Human Cancers-Response. Clin Cancer Res. 2019;25(11):3469-70.
10. Ferrara R, Susini S, Marabelle A. Anti-CTLA-4 Immunotherapy Does Not Deplete FOXP3(+) Regulatory T Cells (Tregs) in Human Cancers-Letter. Clin Cancer Res. 2019;25(11):3468.
11. Galon J, Bruni D. Approaches to treat immune hot, altered and cold tumours with combination immunotherapies. Nature reviews Drug discovery. 2019;18(3):197-218.
12. Vigano S, Alatzoglou D, Irving M, Menetrier-Caux C, Caux C, Romero P, et al. Targeting Adenosine in Cancer Immunotherapy to Enhance T-Cell Function. Frontiers in immunology. 2019;10:925.
13. Cekic C, Linden J. Purinergic regulation of the immune system. Nat Rev Immunol. 2016;16(3):177-92.
14. Zelenay S, van der Veen AG, Bottcher JP, Snelgrove KJ, Rogers N, Acton SE, et al. Cyclooxygenase-Dependent Tumor Growth through Evasion of Immunity. Cell. 2015;162(6):1257-70.
15. Boison D, Yegutkin GG. Adenosine Metabolism: Emerging Concepts for Cancer Therapy. Cancer cell. 2019;36(6):582-96.
16. Beavis PA, Stagg J, Darcy PK, Smyth MJ. CD73: a potent suppressor of antitumor immune responses. Trends Immunol. 2012;33(5):231-7.
17. Ohta A, Gorelik E, Prasad SJ, Ronchese F, Lukashev D, Wong MK, et al. A2A adenosine receptor protects tumors from antitumor T cells. Proc Natl Acad Sci U S A. 2006;103(35):13132-7.
18. Leone RD, Sun IM, Oh MH, Sun IH, Wen J, Englert J, et al. Inhibition of the adenosine A2a receptor modulates expression of T cell coinhibitory receptors and improves effector

function for enhanced checkpoint blockade and ACT in murine cancer models. Cancer immunology, immunotherapy : CII. 2018;67(8):1271-84.
19. Young A, Ngiow SF, Barkauskas DS, Sult E, Hay C, Blake SJ, et al. Co-inhibition of CD73 and A2AR Adenosine Signaling Improves Anti-tumor Immune Responses. Cancer cell. 2016;30(3):391-403.
20. Cekic C, Linden J. Adenosine A2A receptors intrinsically regulate CD8+ T cells in the tumor microenvironment. Cancer Res. 2014;74(24):7239-49.
21. Willingham SB, Ho PY, Hotson A, Hill C, Piccione EC, Hsieh J, et al. A2AR Antagonism with CPI-444 Induces Antitumor Responses and Augments Efficacy to Anti-PD-(L)1 and Anti-CTLA-4 in Preclinical Models. Cancer immunology research. 2018;6(10):1136-49.
22. Avery L, Filderman J, Szymczak-Workman AL, Kane LP. Tim-3 co-stimulation promotes short-lived effector T cells, restricts memory precursors, and is dispensable for T cell exhaustion. Proc Natl Acad Sci U S A. 2018;115(10):2455-60.
23. Zang K, Hui L, Wang M, Huang Y, Zhu X, Yao B. TIM-3 as a Prognostic Marker and a Potential Immunotherapy Target in Human Malignant Tumors: A Meta-Analysis and Bioinformatics Validation. Front Oncol. 2021;11:579351.
24. Acharya N, Sabatos-Peyton C, Anderson AC. Tim-3 finds its place in the cancer immunotherapy landscape. J Immunother Cancer. 2020;8(1).
25. de Mingo Pulido A, Gardner A, Hiebler S, Soliman H, Rugo HS, Krummel MF, et al. TIM-3 Regulates CD103(+) Dendritic Cell Function and Response to Chemotherapy in Breast Cancer. Cancer cell. 2018;33(1):60-74 e6.
26. Ferris RL, Lu B, Kane LP. Too much of a good thing? Tim-3 and TCR signaling in T cell exhaustion. J Immunol. 2014;193(4):1525-30.
27. Janicki CN, Jenkinson SR, Williams NA, Morgan DJ. Loss of CTL function among high-avidity tumor-specific CD8+ T cells following tumor infiltration. Cancer Res. 2008;68(8):2993-3000.
28. Jenkinson SR, Williams NA, Morgan DJ. The role of intercellular adhesion molecule-1/LFA-1 interactions in the generation of tumor-specific CD8+ T cell responses. J Immunol. 2005;174(6):3401-7.
29. Keddie JR, Poucher SM, Shaw GR, Brooks R, Collis MG. In vivo characterisation of ZM 241385, a selective adenosine A2A receptor antagonist. Eur J Pharmacol. 1996;301(1-3):107-13.
30. Poucher SM, Keddie JR, Singh P, Stoggall SM, Caulkett PW, Jones G, et al. The in vitro pharmacology of ZM 241385, a potent, non-xanthine A2a selective adenosine receptor antagonist. British journal of pharmacology. 1995;115(6):1096-102.
31. Phillis JW. The selective adenosine A2 receptor agonist, CGS 21680, is a potent depressant of cerebral cortical neuronal activity. Brain Res. 1990;509(2):328-30.
32. Hodi FS, Chiarion-Sileni V, Gonzalez R, Grob JJ, Rutkowski P, Cowey CL, et al. Nivolumab plus ipilimumab or nivolumab alone versus ipilimumab alone in advanced melanoma (CheckMate 067): 4-year outcomes of a multicentre, randomised, phase 3 trial. Lancet Oncol. 2018;19(11):1480-92.
33. Murakami N, Riella LV. Co-inhibitory pathways and their importance in immune regulation. Transplantation. 2014;98(1):3-14.
34. Buchbinder EI, Desai A. CTLA-4 and PD-1 Pathways: Similarities, Differences, and Implications of Their Inhibition. Am J Clin Oncol. 2016;39(1):98-106.
35. Zeidan AM, Komrokji RS, Brunner AM. TIM-3 pathway dysregulation and targeting in cancer. Expert Rev Anticancer Ther. 2021:1-12.

36. Cekic C, Day YJ, Sag D, Linden J. Myeloid expression of adenosine A2A receptor suppresses T and NK cell responses in the solid tumor microenvironment. Cancer Res. 2014;74(24):7250-9.
37. Wennerberg E, Spada S, Rudqvist NP, Lhuillier C, Gruber S, Chen Q, et al. CD73 Blockade Promotes Dendritic Cell Infiltration of Irradiated Tumors and Tumor Rejection. Cancer immunology research. 2020;8(4):465-78.
38. Cekic C, Sag D, Li Y, Theodorescu D, Strieter RM, Linden J. Adenosine A2B receptor blockade slows growth of bladder and breast tumors. J Immunol. 2012;188(1):198-205.
39. Cekic C, Sag D, Day YJ, Linden J. Extracellular adenosine regulates naive T cell development and peripheral maintenance. J Exp Med. 2013;210(12):2693-706.
40. Jenner P. An overview of adenosine A2A receptor antagonists in Parkinson's disease. Int Rev Neurobiol. 2014;119:71-86.
41. Wang L, Fan J, Thompson LF, Zhang Y, Shin T, Curiel TJ, et al. CD73 has distinct roles in nonhematopoietic and hematopoietic cells to promote tumor growth in mice. J Clin Invest. 2011;121(6):2371-82.
42. Sands WA, Palmer TM. Adenosine receptors and the control of endothelial cell function in inflammatory disease. Immunol Lett. 2005;101(1):1-11.
43. Chimote AA, Balajthy A, Arnold MJ, Newton HS, Hajdu P, Qualtieri J, et al. A defect in KCa3.1 channel activity limits the ability of CD8(+) T cells from cancer patients to infiltrate an adenosine-rich microenvironment. Sci Signal. 2018;11(527).
44. Leone RD, Emens LA. Targeting adenosine for cancer immunotherapy. J Immunother Cancer. 2018;6(1):57.
45. Beavis PA, Milenkovski N, Henderson MA, John LB, Allard B, Loi S, et al. Adenosine Receptor 2A Blockade Increases the Efficacy of Anti-PD-1 through Enhanced Antitumor T-cell Responses. Cancer immunology research. 2015;3(5):506-17.
46. Laudanna C, Campbell JJ, Butcher EC. Elevation of intracellular cAMP inhibits RhoA activation and integrin-dependent leukocyte adhesion induced by chemoattractants. J Biol Chem. 1997;272(39):24141-4.
47. Zeidan A, Gan XT, Thomas A, Karmazyn M. Prevention of RhoA activation and cofilin-mediated actin polymerization mediates the antihypertrophic effect of adenosine receptor agonists in angiotensin II- and endothelin-1-treated cardiomyocytes. Molecular and cellular biochemistry. 2014;385(1-2):239-48.
48. Tasken K, Ruppelt A. Negative regulation of T-cell receptor activation by the cAMP-PKA-Csk signalling pathway in T-cell lipid rafts. Front Biosci. 2006;11:2929-39.
49. Rangachari M, Zhu C, Sakuishi K, Xiao S, Karman J, Chen A, et al. Bat3 promotes T cell responses and autoimmunity by repressing Tim-3-mediated cell death and exhaustion. Nat Med. 2012;18(9):1394-400.
50. Basingab FS, Ahmadi M, Morgan DJ. IFNgamma-Dependent Interactions between ICAM-1 and LFA-1 Counteract Prostaglandin E2-Mediated Inhibition of Antitumor CTL Responses. Cancer immunology research. 2016;4(5):400-11.
51. Chan ESL, Montesinos MC, Fernandez P, Desai A, Delano DL, Yee H, et al. Adenosine A(2A) receptors play a role in the pathogenesis of hepatic cirrhosis. British Journal of Pharmacology. 2006;148(8):1144-55.
52. Schindelin J, Arganda-Carreras I, Frise E, Kaynig V, Longair M, Pietzsch T, et al. Fiji: an open-source platform for biological-image analysis. Nat Methods. 2012;9(7):676-82.
53. Legland D, Arganda-Carreras I, Andrey P. MorphoLibJ: integrated library and plugins for mathematical morphology with ImageJ. Bioinformatics. 2016;32(22):3532-4.

54. Edelsbrunner H, Kirkpatrick DG, Seidel R. On the Shape of a Set of Points in the Plane. Ieee T Inform Theory. 1983;29(4):551-9.
55. Enderling H, Chaplain MA, Anderson AR, Vaidya JS. A mathematical model of breast cancer development, local treatment and recurrence. J Theor Biol. 2007;246(2):245-59.
56. Enderling H, Chaplain MA. Mathematical modeling of tumor growth and treatment. Curr Pharm Des. 2014;20(30):4934-40.
57. Loizides C, Iacovides D, Hadjiandreou MM, Rizki G, Achilleos A, Strati K, et al. Model-Based Tumor Growth Dynamics and Therapy Response in a Mouse Model of De Novo Carcinogenesis. PLoS One. 2015;10(12):e0143840.

Acknowledgement
We acknowledge the University of Bristol Flow Cytometry Facility with Andrew Herman and Lorena Sueiro-Ballesteros and the Wolfson BioImaging Facility with Katie Jepson for experimental support, Alan Hedges for statistical advice, and Mick Bailey for contributions to the principal component analysis.

This work was supported by grants from the Wellcome Trust via the University of Bristol Elizabeth Blackwell Institute (Wellcome Trust ISSF2 grant 105612/Z/14/Z to G.L.E.) and the Wellcome Trust (201254/Z/16/Z/ to G.L.E.). G.L.E is also supported as an associate of the GW4-CAT clinical academic training scheme.

Author contributions
G.L.E. designed and carried out experiments, analyzed data and wrote the paper. C.C.W.W. designed and carried out experiments and analyzed data. R.A designed and carried out experiments and analyzed data. E.M. designed and carried out experiments and analyzed data. H.A. designed and carried out experiments and analyzed data. S.J.C. designed methods for image analysis, G.G. carried out experiments and analyzed data. C.W. designed and carried out experiments, analyzed data and wrote the paper. D.J.M. designed and carried out experiments, analyzed data and wrote the paper.

Competing interests
The authors declare no competing interests

Supplementary information
Supplementary figures
Supplementary image analysis workflow files